Supplementary Information

Biomineralization synthesis of a near-infrared fluorescent nanoprobe for direct glucose sensing in whole blood

Honghua Deng, Huiqiong Liu, Wenyuan Kang, Chunyang Lei*, Zhou Nie, Yan Huang*, Shouzhuo Yao

State Key Laboratory of Chemo/Biosensing and Chemometrics, College of Chemistry and Chemical Engineering, Hunan Provincial Key Laboratory of Biomacromolecular Chemical Biology, Hunan University, Changsha 410082, P. R. China.

Fax: +86-731-88821848; Tel: +86-731-88821626;

E-mail: huangyan.hnu@gmail.com; cylei@hnu.edu.cn.

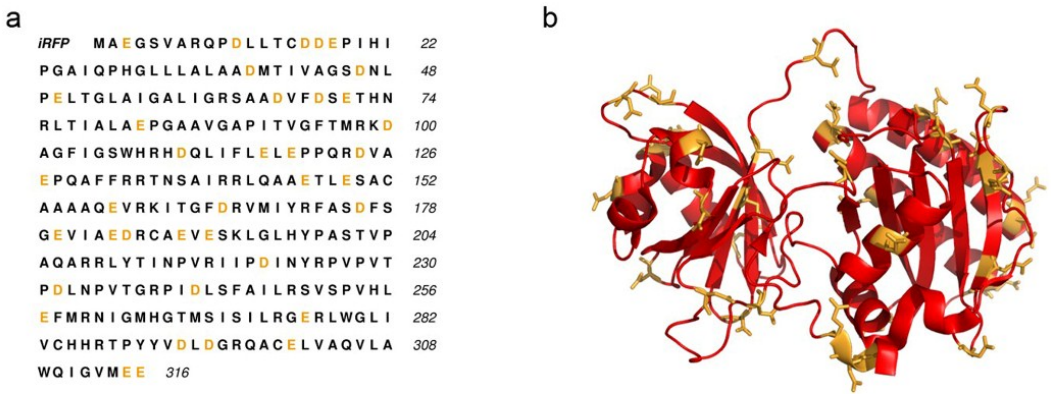

Figure S1. (a) Amino acid sequence and (b) the overall structure of iRFP based on the structure of parental RpBphP2 (PDB: 4E04). Acidic residues containing carboxyl group in iRFP are labeled with orange.

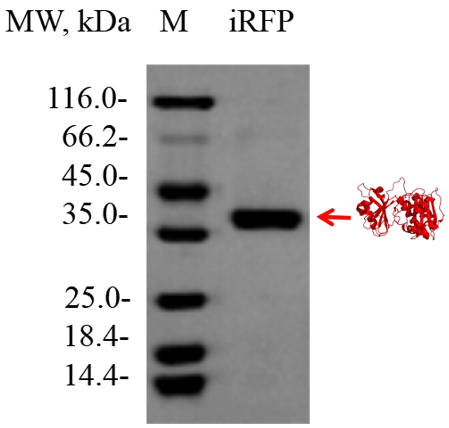

Figure S2. Analysis of purified iRFP by SDS-PAGE (12%).

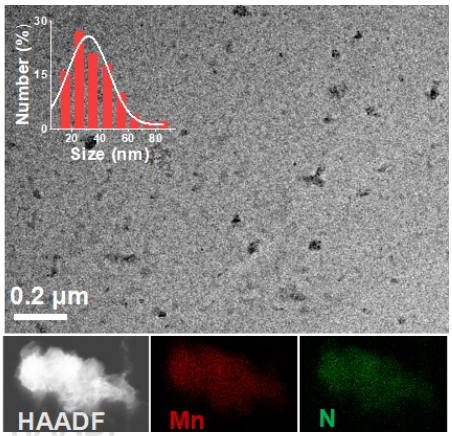

Figure S3. TEM image of iRMs and the corresponding mapping images.

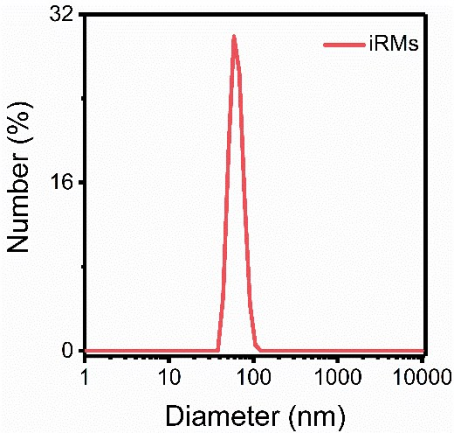

Figure S4. Hydrodynamic diameters of iRMs measured by dynamic light scattering (DLS).

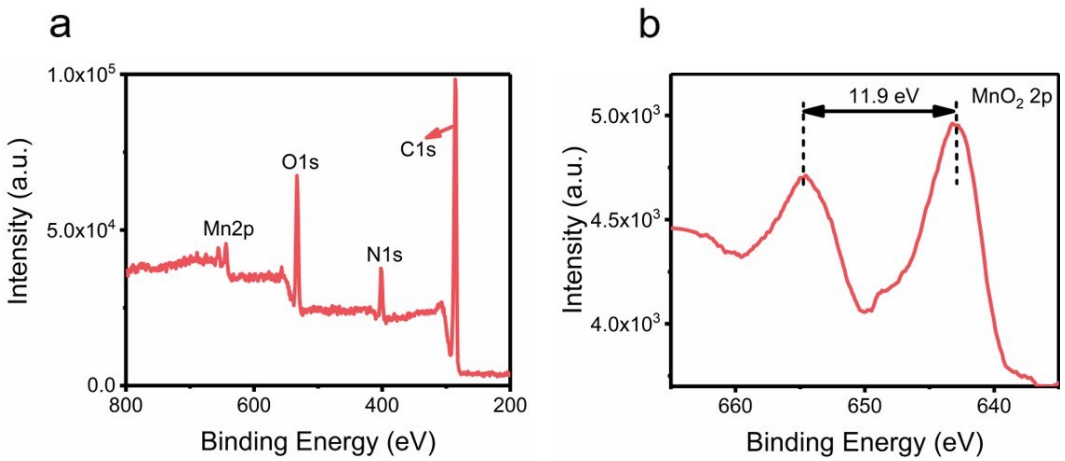

Figure S5. (a) XPS spectra of iRMs. The survey spectrum showed the C, N, O, and Mn peaks. (b) Mn 2p XPS spectrum of iRMs.

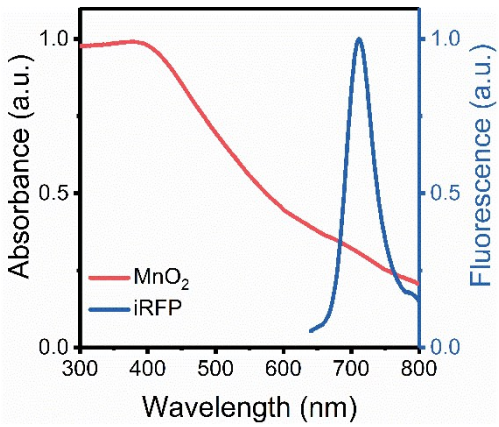

Figure S6. UV-vis absorption spectrum of MnO_2 nanoparticles (red line) and the emission spectrum of iRFP under excitation of 675nm (blue line).

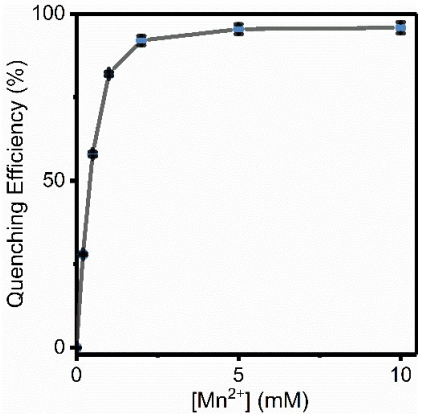

Figure S7. Fluorescence quenching efficiency of iRFP at different concentrations of Mn^{2+} ion during the biomineralization. The iRFP concentration is 0.76 mg·mL^{-1}.

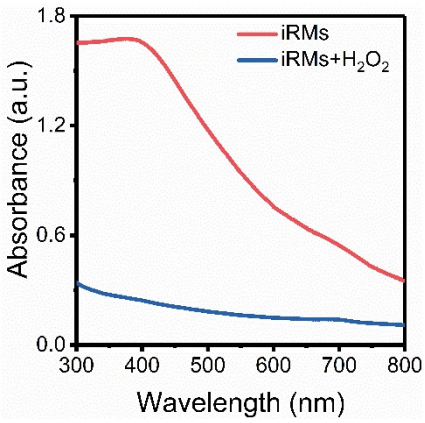

Figure S8. UV-vis absorption spectra of iRMs (red line) and iRMs after reaction with 2 mM H_2O_2 (blue line) in MES buffer (10 mM MES, 100 mM NaCl and pH 6.5).

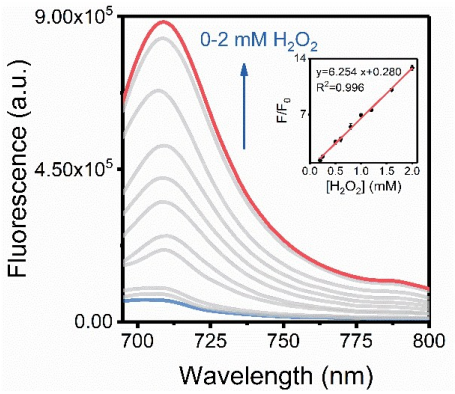

Figure S9. Fluorescence spectra of iRMs with different concentrations of H_2O_2 (0-5 mM) in MES buffer (10 mM MES, 100 mM NaCl and pH 6.5). Inset shows the linear correlation of F/F_0 to H_2O_2 concentration ranging from 0.2 to 2 mM.

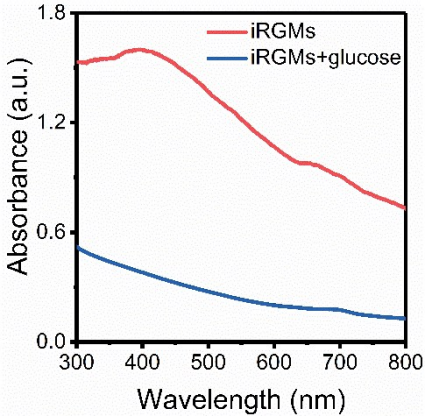

Figure S10. UV-vis absorption spectrum of iRGMs (red line) and iRGMs after reaction with 2mM glucose (blue line) in MES buffer (10 mM MES, 100 mM NaCl and pH 6.5).

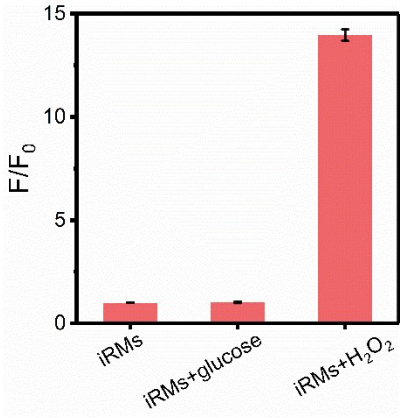

Figure S11. Fluorescence responses of iRMs toward H_2O_2 (2.0 mM) and glucose (2.0 mM).

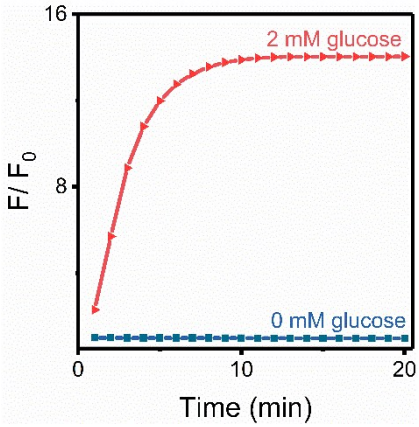

Figure S12. The kinetic fluorescence response signal of iRGMs to glucose at 2.0 mM.

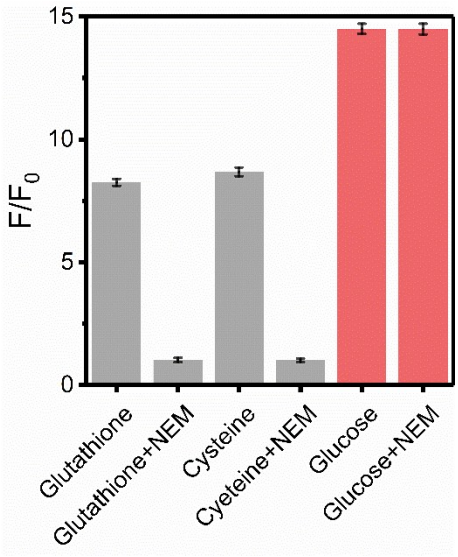

Figure S13. Fluorescence response signal of the nanoprobe to biothiols at room temperature. Glucose, GSH and Cys, 2.0 mM; NEM, 6.0 mM.

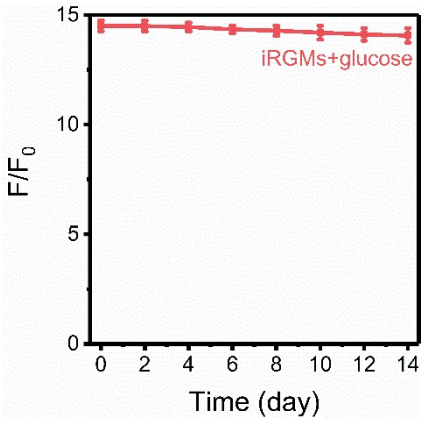

Figure S14. Fluorescence responses of iRGMs with different storage times (stored at 4 ℃) toward glucose (2 mM).

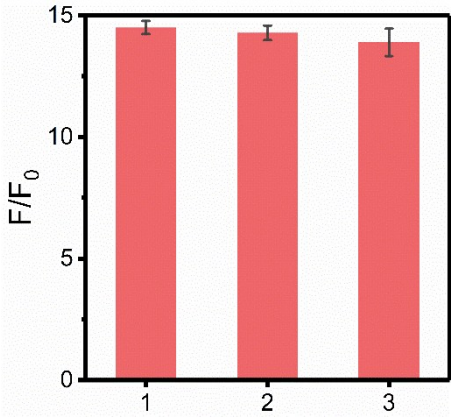

Figure S15. Fluorescence responses of three batches of iRGMs nanoparticles toward glucose (2 mM).

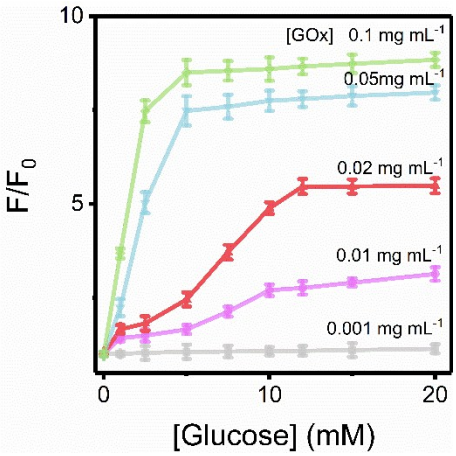

Figure S16. Fluorescence response signals of iRGMs to glucose. The iRGMs contain different concentrations of GOx (0.001, 0.01, 0.02, 0.05, 0.1 mg·mL^{-1}). Error bars represent the standard deviation from three repetitive experiments.

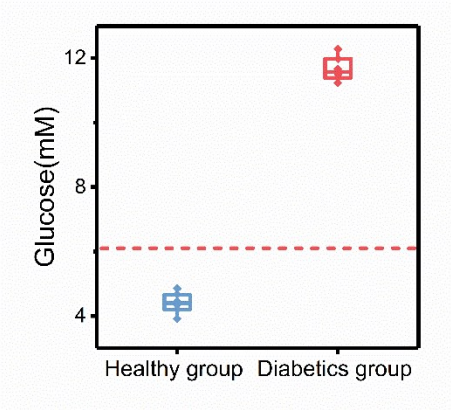

Figure S17. Quantification of glucose in whole blood samples from healthy and diabetic mice.

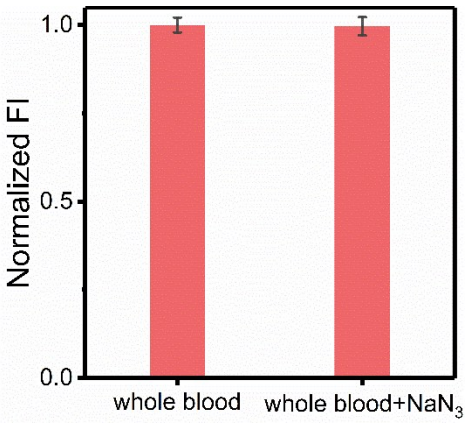

Figure S18 Fluorescence intensity of iRGMs nanoparticles toward whole blood samples with and without the addition of sodium azide (50 μM).

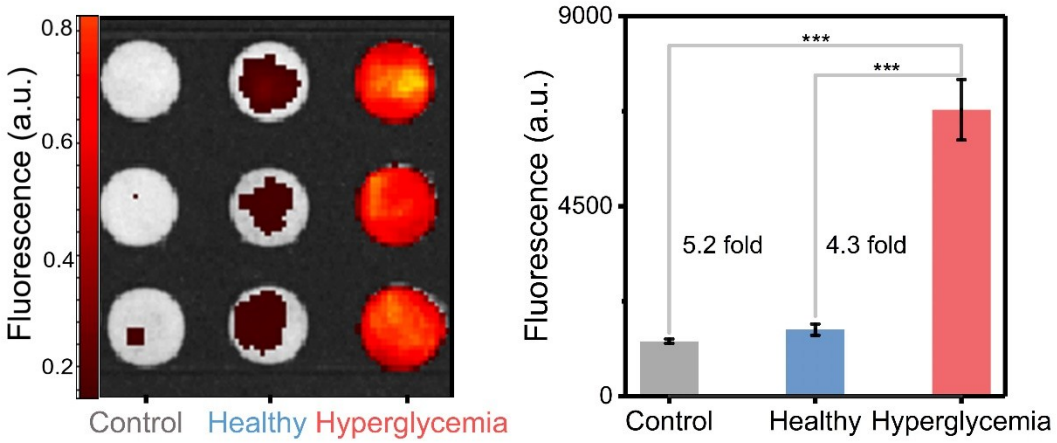

Figure S19 NIR fluorescence image of whole blood samples analysed by the iRGMs-based paper device. Semiquantitative results of the average intensities in NIR image. Data points represent mean ± SD (n = 3). ***p < 0.001.

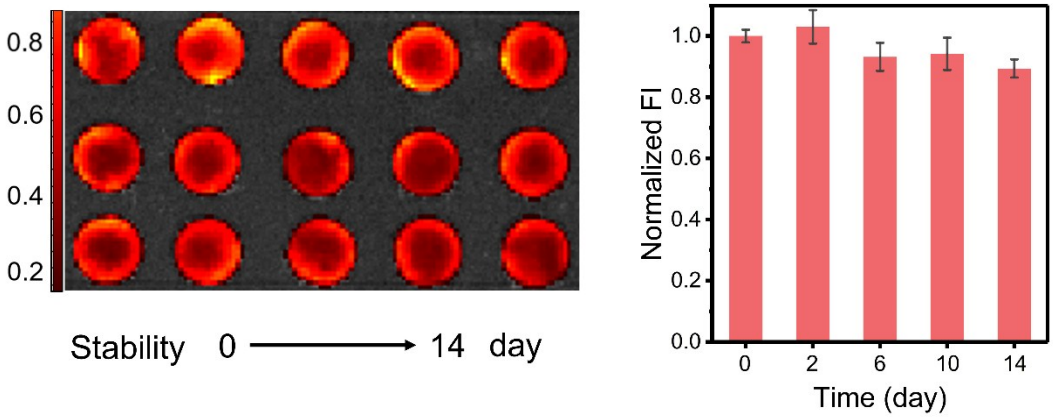

Figure S20 NIR fluorescence image of whole blood sample (8 mM glucose) analysed by the iRGMs-based paper device with different storage times (stored at 4 ℃). The fluorescence intensity of the paper device toward the same blood sample.